ISSN 1064-2269, Journal of Communications Technology and Electronics, 2013, Vol. 58, No. 5, pp. 417–428. © Pleiades Publishing, Inc., 2013.
Original Russian Text © A.P. Anyutin, A.D. Shatrov, 2013, published in Radiotekhnika i Elektronika, 2013, Vol. 58, No. 5, pp. 464–476.

ELECTRODYNAMICS AND WAVE PROPAGATION

The Wave Theory of Infinite and Finite Veselago Lenses

A. P. Anyutin[a] and A. D. Shatrov[b]

[a] *Russian New University, ul. Radio 22, Moscow, 105005 Russia*
e-mail: anioutine@mail.ru

[b] *Institute of Radio Engineering and Electronics, Russian Academy of Sciences (Fryazino Branch), pl. Vvedenskogo 1, Fryazino, Moscow oblast, 141190 Russia*
e-mail: korip@ms.ire.rssi.ru

Received July 17, 2012

Abstract—The results of investigation of the problem of cylindrical wave scattering by infinite and finite Veslago lenses are discussed. The problem is considered in a rigorous electrodynamic formulation. It is shown that the superfocusing effect is impossible in an ideal Veselago lens. It is reported that the near-field structures observed in the case of diffraction of a cylindrical wave by an electrically thick lens and an electrically thin lens are substantially different.

DOI: 10.1134/S1064226913040037

INTRODUCTION

The problem of diffraction (scattering) of electromagnetic waves by compact metamaterial (i.e., artificial-medium) bodies is one of the most intensely discussed problems in the modern scientific literature. Note that, at present, the term *metamaterial* is employed in several meanings. Initially, the term *metamaterial* was introduced in 2004 [1] for a medium whose permittivity ε and permeability μ are simultaneously negative, $\varepsilon < 0$, $\mu < 0$. As is known, in earlier study [2], such a medium was called a medium with negative refraction. Later, in the studies devoted to creation of a medium with a negative permittivity ($\varepsilon < 0$) and a negative permeability ($\mu < 0$), the term *metamaterial* was also used.

The problem of field focusing by a plane layer of a medium with the permittivity and permeability that are simultaneously negative is regarded as a special one. Veselago showed [2] that a plane layer of a medium with $\varepsilon = -1$, $\mu = -1$ provides for ideal (in terms of geometric optics (GO)) focusing of transmitted and refracted GO rays. In the case of ideal focusing, all of the transmitted (refracted) GO rays merge at a single point. In other words, a plane layer of such a medium transforms the divergent front of the incident cylindrical wave into the convergent front of the transmitted wave. In the modern scientific literature, this plane layer is called an ideal Veselago lens. In Pendry's study [1], it is stated that the Veselago lens provides for an ideal image that is identical to the source and contains details with dimensions smaller than the wavelength.

Note that, in most theoretical studies, the model of an electrically thick plane layer of an infinite length is considered. The field of a cylindrical (spherical) wave transmitted through such a lens is analyzed on the basis of the field representation in the form of an integral over plane (cylindrical) waves and the subsequent asymptotic calculation of this integral by means of the stationary phase method. As is known, this analysis yields results equivalent to those obtained by means of the GO method. In addition, the researchers use the ray description of the field in the small-angle approximation, the GO approximation taking into account the transmission of GO rays through the layer without their rereflection by the layer boundaries, and the thin-layer or Kirchhoff approximation. Actually, this means that various versions of approximate (asymptotic) methods are used. The use of rigorous numerical methods for the solution of problems of electromagnetic wave diffraction by compact metamaterial bodies was restricted to the case when a body's dimensions were commensurable with the wavelength [3–5].

The first results of numerical calculation of the field structure in the focus region of a finite Veselago lens were obtained in [7] on the basis of the solution of the problem in the rigorous formulation, similar results were obtained for an infinite plane Veselago lens [6, 10, 12].

The discussed research area is topical, because, until now, we see publications where it is erroneously stated that the Veselago lens provides for ideal focusing, i.e., for the field spatial localization in a volume whose dimension is not limited by wavelength λ, and the dimension of this volume is related with the source size only.

1. AN INFINITE VESELAGO LENS

Consider the 2D problem of excitation of a metamaterial plate with negative relative permittivity ε

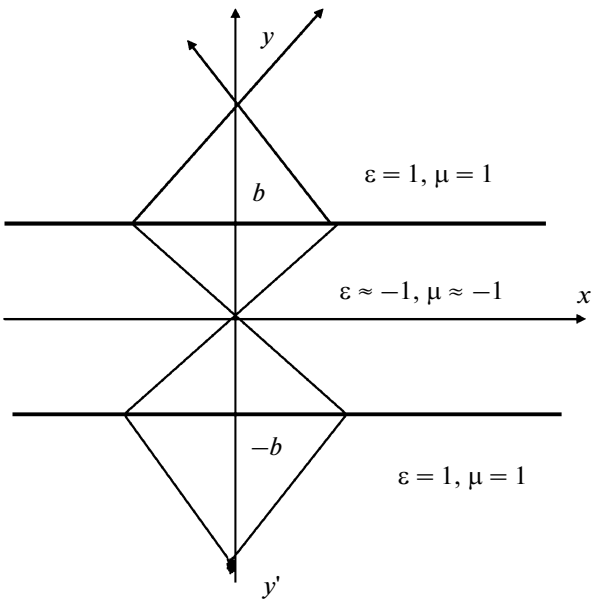

Fig. 1. Infinite Veselago lens.

and permeability μ by a magnetic current filament located at the point $(0, y')$ (Fig. 1). Let us investigate the case of the TM polarization, when 2D scalar field $U(x, y)$ has the meaning of the H_z component of the electromagnetic field. Function $U(x, y)$ must satisfy the inhomogeneous Helmholtz equation

$$\frac{\partial^2 U(x,y)}{\partial x^2} + \frac{\partial^2 U(x,y)}{\partial y^2} + k^2\varepsilon(y)\mu(y)U(x,y) = 2\pi\delta(x)\delta(y-y'), \quad y' < -b, \tag{1}$$

where

$$\varepsilon(y) = \begin{cases} \varepsilon, & |y| < b \\ 1, & |y| > b \end{cases}, \quad \mu(y) = \begin{cases} \mu, & |y| < b \\ 1, & |y| > b \end{cases}, \quad k = 2\pi/\lambda. \tag{2}$$

Function $U(x, y)$ must also satisfy the boundary conditions at $y = \pm b$

$$U(x,-b-0) = U(x,-b+0), U(x,b-0) = U(x,b+0),$$
$$\frac{\partial}{\partial y}U(x,-b-0) = \frac{1}{\varepsilon}\frac{\partial}{\partial y}U(x,-b+0),$$
$$\frac{1}{\varepsilon}\frac{\partial}{\partial y}U(x,b-0) = \frac{\partial}{\partial y}U(x,b+0), \tag{3}$$

and the radiation conditions. The solution in the form of the Fourier integral

$$U(x,y) = \int_{-\infty}^{\infty} A(y,h)\exp\{-ihx\}dh \tag{4}$$

to the problem formulated above is well known and presented in many monographs and studies (see, e.g., [19–21]).

For the layer parameters $\varepsilon = \mu = -1$, representation (4) can effectively be applied for calculating the field only in the case when the distance between the source and the plate's nearest boundary $y = -b$ is larger than the plate's thickness ($y' < -3b$). When the source is located at a smaller distance ($-3b < y' < -b$), then, according to the GO concepts, two focuses are formed in the field: one is located beyond the plate ($x = 0$, $y = y' + 4b$) and the other is inside it ($x = 0$, $y = -y' - 2b$) [2]. The focuses are situated symmetrically with respect to the boundary $y = b$. In this case, integral (4) diverges in the strip between two focal planes $|y - b| < y' + 3b$. This means that, for these parameters of the layer, the excitation problem has no solution. For the problem to have a solution, it is necessary to consider a layer with small deviations of quantities ε and μ from minus unity or introduce a medium loss. Note that, because of the slow convergence of integral (4), this method is not efficient for calculating the field.

The spectral method is more suitable for numerical and analytical investigations. It is based on the field decomposition in the eigenwaves of discrete and continuous spectra. Functions $\psi(y, \alpha)$ of the continuous spectrum are solutions to the ordinary differential equation

$$\varepsilon\frac{d}{dy}\left(\frac{1}{\varepsilon}\frac{d\psi}{dy}\right) + k^2(\varepsilon\mu - 1)\psi + \alpha^2\psi = 0. \tag{5}$$

Function $\psi(y, \alpha)$ must be continuous along with its weighted derivative $\frac{1}{\varepsilon(y)}\frac{d\psi(y,\alpha)}{dy}$ on the layer boundaries. In the calculation below, it is convenient to use two functions $\psi_1(y, \alpha)$ and $\psi_2(y, \alpha)$ of the continuous spectrum that have the following form beyond the layer:

$$\psi_1(y,\alpha) = \exp[-i\alpha(y-b)], \quad y > b,$$
$$\psi_2(y,\alpha) = \exp[i\alpha(y+b)], \quad y < -b. \tag{6}$$

Let $W(\alpha)$ denote the Wronskian of these functions:

$$W(\alpha) = \frac{1}{\varepsilon}\left(\psi_2\frac{d\psi_1}{dy} - \psi_1\frac{d\psi_2}{dy}\right). \tag{7}$$

Functions $\psi_1(y, \alpha)$ and $\psi_2(y, \alpha)$, where parameter α takes arbitrary real values, exhibit the following biorthogonality property:

$$\int_{-\infty}^{\infty}\frac{1}{\varepsilon(y)}\psi_1(y,\alpha)\psi_2(y,\alpha')dy = N(\alpha)\delta(\alpha-\alpha'), \tag{8}$$

where

$$N(\alpha) = \frac{\pi i}{\alpha}W(\alpha). \tag{9}$$

In the considered problem, in addition to continuous spectrum waves, there are an infinite number of discrete spectrum waves. The transverse wave numbers of these waves are found as the roots of the equation

$$W(\alpha) = 0, \tag{10}$$

that are located in the lower half-plane, $\mathrm{Im}\,\alpha_m < 0$. We denote the transverse distributions of the eigenmode fields $\psi_m(y)$. These functions are determined as follows:

$$\psi_m(y) = \psi_1(y, \alpha_m) = \pm\psi_2(y, \alpha_m). \quad (11)$$

Norm N_m of discrete spectrum functions is coupled with Wronskian $W(\alpha)$ through the formula

$$N_m = \int_{-\infty}^{\infty} \frac{1}{\varepsilon(y)} \psi_m^2(y) dy = \pm \frac{1}{2\alpha_m} \frac{dW}{d\alpha}\bigg|_{\alpha=\alpha_m}. \quad (12)$$

The upper and lower signs in (11) and (12) refer to even and odd functions $\psi_m(y)$, respectively.

The completeness and orthogonality of the eigenwaves of the continuous and discrete spectra enables us to obtain a solution to the diffraction problem in the form

$$U(x, y) = U_1(x, y) + U_2(x, y), \quad (13)$$

where $U_1(x, y)$ and $U_2(x, y)$ are the wave fields of the continuous and discrete spectra. When $y > y'$, we have [2]

$$U_1(x, y) = \int_{-\infty}^{\infty} \frac{\psi_1(y, \alpha)\psi(y', \alpha)}{-2ih(\alpha)N(\alpha)} \exp\left[-ih(\alpha)|x|\right] d\alpha, \quad (14)$$

where $h(\alpha) = \sqrt{k^2 - \alpha^2}$. Here, $h > 0$ when $|\alpha| < k$ and $\mathrm{Im}\,h < 0$ when $|\alpha| > k$.

The contribution of the discrete spectrum waves is determined from the formula [22]

$$U_2(x, y) = \sum_{m=-\infty}^{\infty} \frac{1}{-2ih_m N_m} \psi_m(y)\psi_m(y') \exp\left(-ih_m|x|\right), \quad (15)$$

where $h_m = \sqrt{k^2 - \alpha_m^2}$ and $\mathrm{Im}\,h_m < 0$ for complex waves.

For undamped eigenwaves, the sign of propagation constant h_m should coincide with the sign of norm N_m. This excludes the power influx from infinity.

In contrast to Fourier integral (4), the spectral decomposition explicitly contains the contribution of surface waves, which play an important role in the field formation near the plate. Therefore, the spectral representation proves to be more suitable for investigating the properties of a thin Veselago lens when parameters ε and μ are close to minus unity. Note that the spectral decomposition of the field can be obtained from Fourier integral (4) with the help of a special deformation of the integration contour in the complex plane of h (see, e.g., [23]).

When the norm of a certain surface wave vanishes,

$$N_m = 0, \quad (16)$$

then, decomposition (15) has no meaning. It follows from (12) that, in this case, quantity α_m is a multiple root of function $W(\alpha)$.

The undamped surface waves

$$U_m(x, y) = \psi_m(y) \exp(-ih_m x), \quad (17)$$

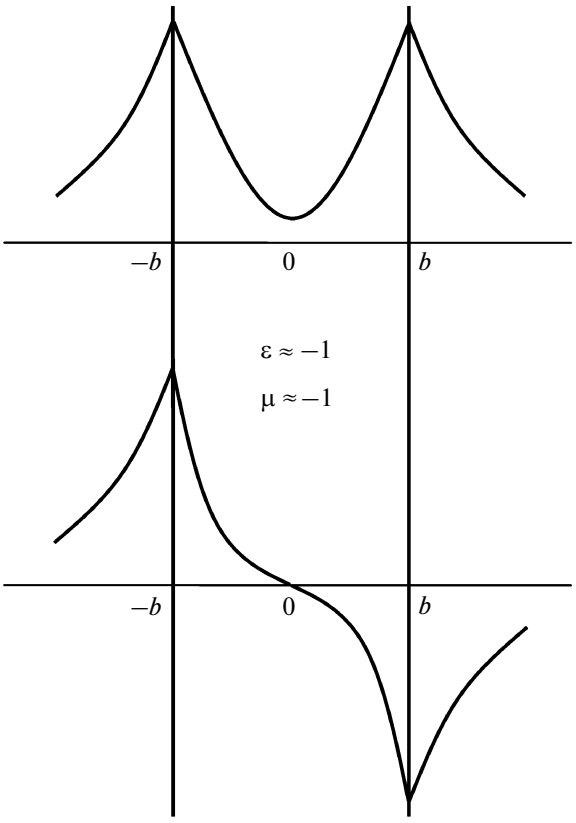

Fig. 2. Field distribution in even and odd surface waves.

can propagate over the plate. These waves have real propagation constant h_m and imaginary wave numbers α_m. Functions $\psi_m(y)$ corresponding to even and odd waves are schematically shown in Fig. 2.

The total power transferred by a surface wave in the positive direction of the x axis is proportional to the quantity $h_m N_m$. When $N_m > 0$ ($N_m < 0$), the wave is forward (backward). The direction of the phase velocity of a forward wave coincides with the direction of the total power transfer. For a backward wave, these directions are opposite.

Figure 3 shows curves characterizing the relationships between the values of parameters ε and μ such that forward and backward surface waves are doubly degenerate [16]. The solid (dashed) curves correspond to an even (odd) wave. Curves *1–3* correspond to the values kb = 1, 1.25, and 2. Different points on the curves are associated with different wave slowing factors. All of the cusp points of the curves corresponding to the degenerate even wave lie on the vertical straight line $\varepsilon = -1.0363...$ At cusp points, a surface wave is triply degenerate [24]. When layer parameters ε, μ, and kb belong to the corresponding curve, the problem of layer excitation has no solution because of the resonance of the forward and backward surface waves [22].

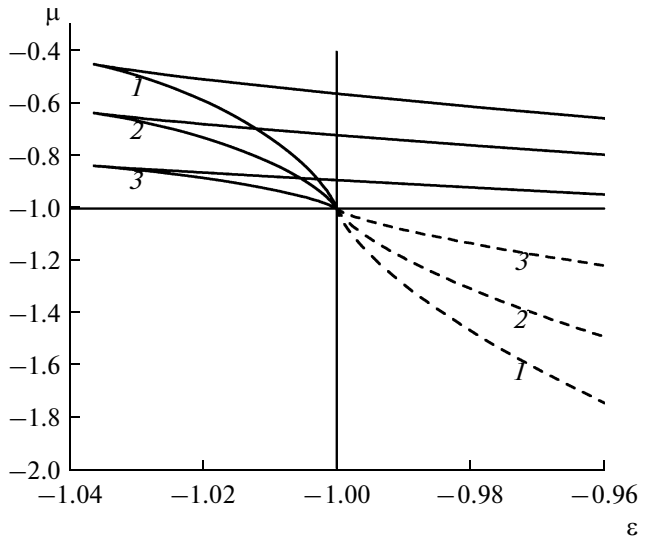

Fig. 3. Constitutive parameters leading to the double degeneration of surface waves.

Evidently, the introduction of a small heat loss removes this problem.

All of the curves from Fig. 3 end at the point (−1, −1). When this point is approached, the wave slowing factor infinitely grows ($h/k \to \infty$) and the fields localize near the layer boundaries. The intersection of all of the curves at the point (−1, −1) means that the calculation of the field near this point is an ill-posed problem. As $\varepsilon \to -1$ and $\mu \to -1$, the field amplitude near the layer boundary infinitely grows and the spatial structure of the field substantially depends on the way in which constitutive parameters ε and μ approach the singular point $\varepsilon = -1$, $\mu = -1$.

In studies [6, 15, 16, 22], the focusing properties of plates are investigated for the case when the constitutive parameters ε and μ approach the singular point so that their values belong to the curve $\varepsilon\mu = 1$. The deviation of the constitutive parameters from the singular point is characterized by real quantity σ:

$$\varepsilon = \frac{\sigma+1}{\sigma-1}, \quad \mu = \frac{\sigma-1}{\sigma+1}, \quad |\sigma| \ll 1. \tag{18}$$

In this case, the functions of the continuous and discrete spectra have a simple form, and expressions (14) and (15) can be studied analytically. Thus, the wave numbers and norms of the discrete spectrum functions are expressed by the formulas

$$2\alpha_m b = i\ln|\sigma| + \pi m, \quad m = 0, \pm 1, \pm 2, \ldots, \tag{19}$$

$$N_m = 4\sigma b \Big/ \left(1 - \sigma^2\right). \tag{20}$$

The index $m = 0$ is associated with a single undamped wave. When $\sigma > 0$, this wave is a forward ($N_0 > 0$) one with the odd distribution of the field

$$\psi_0(y) = \frac{\sin(\alpha_0 y)}{\sin(\alpha_0 b)}, \quad |y| < b. \tag{21}$$

When $\sigma < 0$, this wave is a backward ($N_0 < 0$) one with the even distribution of the field

$$\psi_0(y) = \frac{\cos(\alpha_0 y)}{\cos(\alpha_0 b)}, \quad |y| < b. \tag{22}$$

Field (15) of the discrete spectrum waves exhibits the following properties as $\sigma \to 0$. The field approaches zero when $y' < -3b$ and infinitely grows in the spatial regions adjacent to the layer boundaries ($|y + b| < y' + 3b$, $|y - b| < y' + 3b$) when $-3b < y' < -b$.

In studies [5, 15, 16, 24], the field distributions in the focal plane ($y = y' + 4b$) and on the lens axis ($x = 0$) are investigated for the case when $\sigma \to 0$. It is shown that the superresolution effect, i.e., the situation when the dimension of the spot in the focal plane of the lens is substantially smaller than the wavelength, occurs under the condition

$$|\ln|\sigma|| \gg 2kb. \tag{23}$$

When this condition is fulfilled, the reactive component of the field dominates over its dynamic component in the focal plane. Note that the reactive component is the response of the layer to the point excitation source field component that is described by the integral over plane waves exponentially decaying in the direction of the y axis. The dynamic component is the response to the superposition of propagating plane waves. As $\varepsilon \to -1$ and $\mu \to -1$, this field component remains constant and is described by the Bessel function in the focal planes

$$U(x, -y' - 2b) = U(x, y' + 4b) = \frac{i\pi}{2} J_0(kx). \tag{24}$$

Taking into account that logarithm is a slow function of its argument, we can see that even a slight increase in the layer's thickness $2kb$ necessitates substantial decrease of σ. For example, when the constitutive parameters differ from minus unity by values of about 10^{-4}, the superresolution effect is possible only when the thickness is substantially smaller than the wavelength. Since the source and the focal point are situated in this case near the plate at distances smaller that its thickness, the field can be calculated in the quasi-static approximation [15]. In this situation, the field transmitted through the plate monotonically decreases along the lens axis ($x = 0$), and the field intensity on the plate's boundary exceeds the field intensity at the focus. Therefore, in the case under consideration, there is no focusing in its standard meaning (i.e., focusing understood as the situation when a local maximum of the field intensity is observed at the focal point).

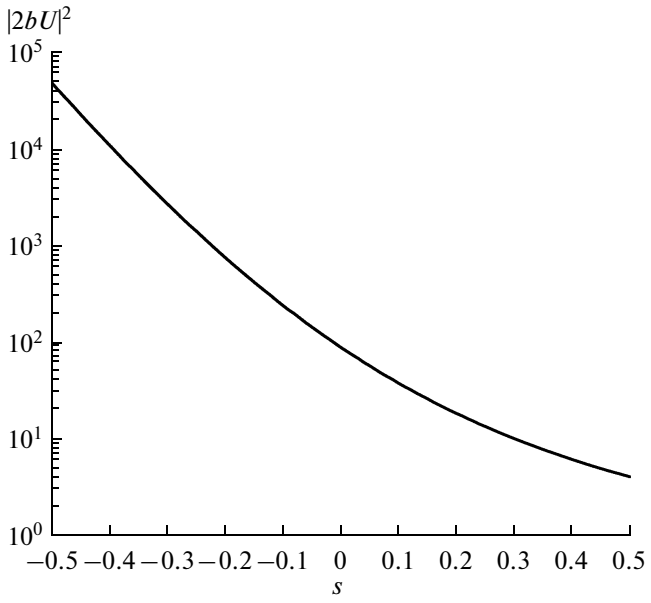

Fig. 4. Field intensity vs. normalized coordinate $s = (y - 2b)/2b$.

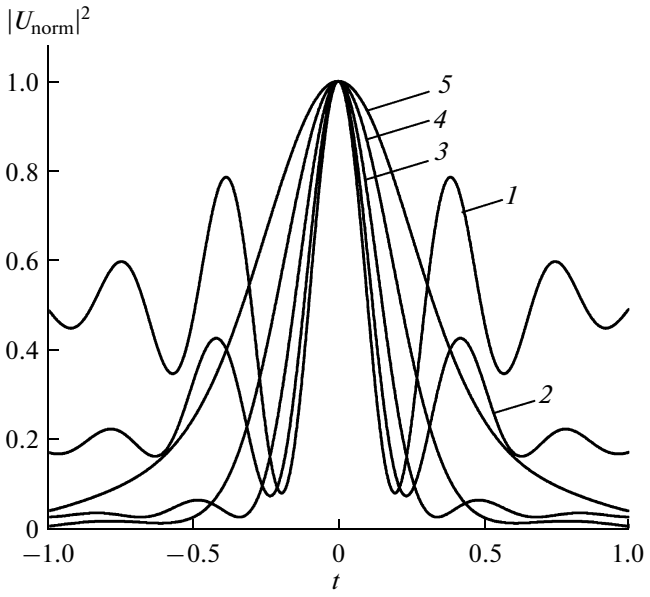

Fig. 5. Field intensity vs. normalized coordinate $t = x/2b$; $s = (1)$ −0.5, −0.25 (*2*), 0 (*3*), 0.25 (*4*), and 0.5 (*5*).

Figure 4 illustrates the variation of the field intensity along the lens axis for $\sigma = -10^{-4}$ and $y' = -2b$. Coordinate y changes from the layer boundary $y = b$ to the point $y = 3b$, which is located symmetrically with respect to the focus. Figure 5 shows field distributions $|U|^2$ normalized to the unit maximum in various sections $y = \text{const}$. It is seen from this figure that, in the sections $y = b$ and $y = 1.5b$, located in front of the focal plane, the fields exhibit an oscillating character with high levels of sidelobes (curves *1* and *2*). In the focal plane ($y = 2b$) and behind it ($y = 2.5b$), the sidelobe level is substantially reduced (curves *3* and *4*). The spot dimension in the focal plane determined from the distance between the neighboring minima of function $|U|^2$ equals

$$D = \frac{4\pi b}{|\ln(|\sigma|)|}. \quad (25)$$

In the case of the TM polarization, for the superresolution effect to be realized, it is more important that parameter ε is close to minus unity, because just this parameter, in contrast to parameter μ, enters the boundary condition for field U [6, 15].

All of the above relationships refer to the case of the TM polarization of the incident field. Obviously, upon the replacement $\varepsilon \to \mu$ and $\mu \to \varepsilon$ (according to the duality principle), these relationships will be valid for the TE polarization of the incident field.

Recall that formula (25) is obtained under the assumption that condition (23) is fulfilled. Taking into account this condition, we have $D \ll \lambda$. The absence of wavelength λ in formula (25) confirms the static character of the field in the neighborhood of the focal point.

Note that formulas (23) and (25) remain meaningful when there is a heat loss in the medium (for example, $\varepsilon = -1 - i\varepsilon''$ and $\mu = -1$). In this case, we should set $\sigma = \varepsilon''/2$ in (23) and (25) [12, 21, 23].

In studies [10, 11], the 3D problem of excitation of an infinite metamaterial layer by an electric dipole was considered. The dipole was oriented in parallel to the layer. For the field, representations in the form of Fourier–Bessel integrals were obtained. These representations were analyzed numerically. Since, in [10, 11], the layer thickness $2kb$ and ε'' did not satisfy condition (23), the superresolution effect was not found. The field at the focus of a thick layer satisfied the Rayleigh criterion.

2. A FINITE VESELAGO LENS

A more realistic model of the Veselago lens is a layer of finite dimensions. In this case, the solution of the diffraction problem necessitates numerical methods. The fields in the Veselago lens are numerically determined with the use of the volume integral equation method [26] and the modified discrete source method (MDSM) [5, 7–9, 13, 14].

2.1. The Calculation Method

The most efficient tool for calculating the fields in the Veselago lens is the MDSM. Let the cylindrical wave

$$U_0(r, \varphi) = H_0^{(2)}(k\sqrt{r^2 + R_0^2 - 2rR_0\cos(\varphi - \varphi_0)}) \quad (26)$$

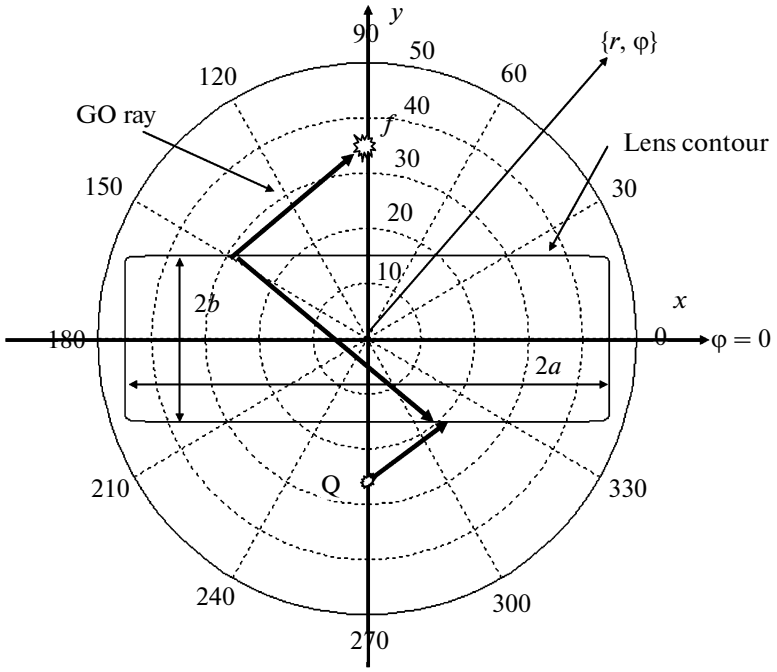

Fig. 6. Finite Veselago lens; f is the focus point and Q is the cylindrical wave source.

interact with a plate of finite dimensions whose contour $\rho_S(\varphi)$ in polar coordinates is described by the equation

$$\rho_S(\varphi) = \frac{1}{\sqrt[p]{[\cos(\varphi)/a]^p + [\sin(\varphi)/b]^p}}. \quad (27)$$

Equating parameter p in (27) to various values, we can change the form of contour $\rho_S(\varphi)$ from a circle (when $p = 2$ and $a = b$) to a rectangle (when $p \gg 1$, e.g., at $p = 20$ and $a \neq b$). The geometry of the problem for $p = 20$ is displayed in Fig. 6.

Expressions (26) and (27) contain the following quantities: $\{r, \varphi\}$ are the coordinates of the observation point in cylindrical coordinates, $\{R_0, \varphi_0\}$ are the coordinates of wave source Q (a magnetic- or electric-current filament) in cylindrical coordinates, and $H_0^{(2)}(\bullet)$ is the zero-order Hankel function of the second kind.

Total field $U(r, \varphi)$ beyond the scatterer can be represented as the superposition of incident wave field (26) and scattered field $U_1(r, \varphi)$

$$U(r,\varphi) = H_0^{(2)}(k\sqrt{r^2 + R_0^2 - 2rR_0\cos(\varphi - \varphi_0)}) + U_1(r,\varphi). \quad (28)$$

The field inside the metamaterial is denoted $U_2(r, \varphi)$.

Fields $U(r, \varphi)$ and $U_2(r, \varphi)$ must satisfy the corresponding Helmholtz equations beyond and inside the plate with contour (27) and the corresponding boundary conditions on contour $\rho_S(\varphi)$ of the plate; i.e., these fields must solve the boundary value problem. We apply the MDSM [27, 28], which allows solving the boundary value problem with a controlled accuracy. In this method, fields $U_1(r, \varphi)$ and $U_2(r, \varphi)$ are represented in the form of the superposition of the fields of auxiliary cylindrical sources located on auxiliary contours $\rho_{\Sigma 1}(\varphi)$ and $\rho_{\Sigma 2}(\varphi)$. Inside and beyond the corresponding contours, this representation automatically satisfies the Helmholtz equations and the Sommerfeld condition.

In the MDSM, the amplitude coefficients for the auxiliary cylindrical sources are found from a solution to the system of linear algebraic equations that follow from the boundary conditions fulfilled at N points of contour $\rho_S(\varphi)$.

The accuracy of a solution to the problem is controlled through calculating the discrepancy of the boundary conditions at the centers of the intervals between the points where the boundary conditions are fulfilled exactly. At these points, the boundary conditions are fulfilled with the worst accuracy [28].

Since the MDSM and its application to a series of problems with a similar configuration of the contour of a scatterer are described in detail in [27, 28], we do not discuss here this method and the technique of its application. However, we note that the results of computation presented below have the maximum discrepancy of the boundary conditions that does not exceed the value $\Delta < 10^{-3}$ for any point of the corresponding contours.

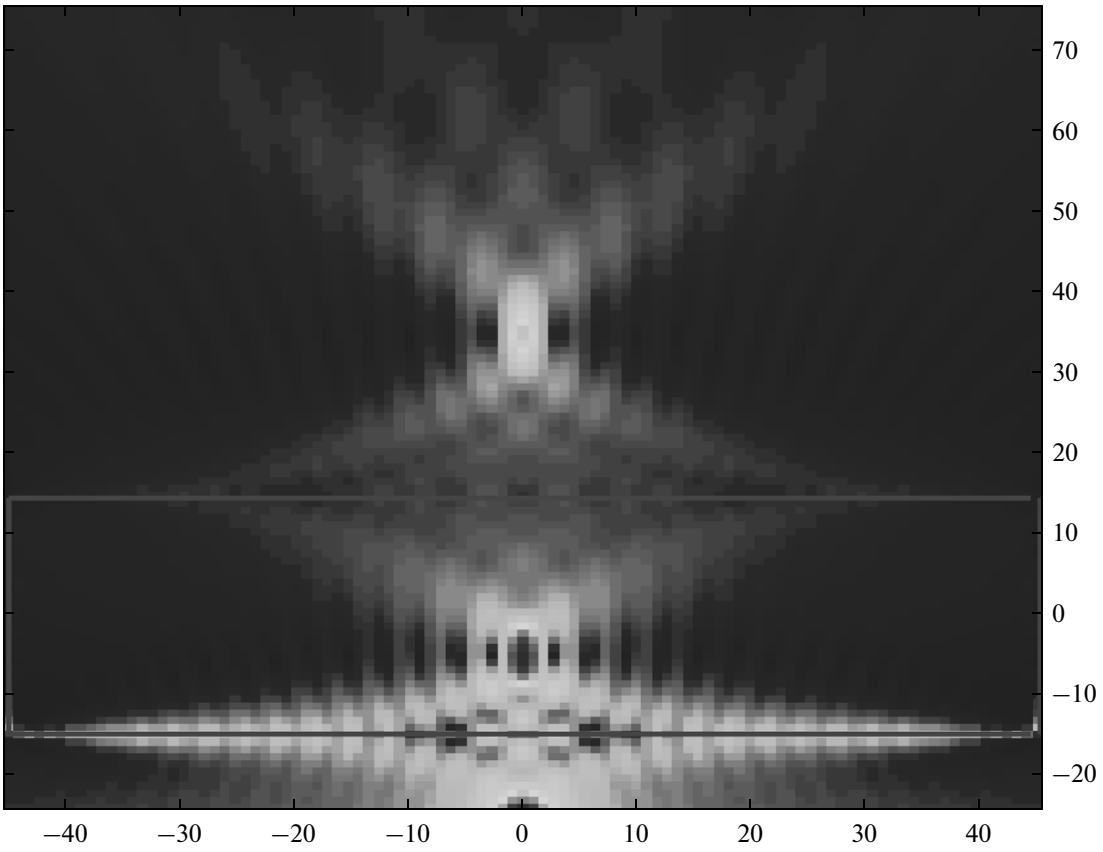

Fig. 7. Spatial distribution of the field amplitude for $\varepsilon = \mu = -1.0001$, $ka = 45$; $kb = 15$; $kR_0 = 25$, and $\varphi_0 = -\pi/2$.

2.2. The Focusing Properties of a Thick Veselago Lens of Finite Dimensions

As compared to a layer of an infinite length (see Fig. 1), in a layer of finite dimensions (see Fig. 6), we observe field rereflections by the narrow butt-ends of the lens, a circumstance that complicates the field structure. Obviously, when length $2a$ of the lens exceeds its thickness $2b$, the electrodynamic properties of this lens are close to the properties of an infinitely long layer.

As in the case of an infinite layer, the results of computation substantially depend on the relationship between the thickness of the layer $2kb$ and the closeness of parameters ε and μ to the singular point $(-1, -1)$ (see (23)). The presence of a heat loss ($\varepsilon'' \neq 0$) determines the theoretical limit of the possible approach to this point. If we restrict the consideration to the value of reachable loss $\varepsilon'' = 10^{-4}$, relationship (23) will be invalid even for the layer thickness exceeding the wavelength. We refer to these lenses as thick ones.

Note that, when the condition $\varepsilon = \mu = -1$ is fulfilled, the problem has no numerical solution, because, the determinant of the system of linear algebraic equations is zero, which matches the results obtained above for an infinite layer.

Let us present typical field distributions in thick lenses for the case of the TE polarization of the incident cylindrical wave. Figure 7 illustrates the general pattern of the focusing effect. In this figure, the spatial field distribution is shown for the case when $\varepsilon = \mu = -1.0001$, $ka = 45$, $kb = 15$, $kR_0 = 25$ and $\varphi_0 = -\pi/2$.

The distribution of the field amplitude along the lens axis is depicted in Fig. 8 for various positions kR_0 of the source. It is seen that the coordinates of the exterior focal point strictly correspond to the GO concepts: $ky = 4kb - kR_0$.

Figure 9 shows the transverse field distribution in various sections $ky = \text{const}$ for a lens with the parameters $\varepsilon = \mu = -1.0001$, $ka = 45$, $kb = 20$, $kR_0 = 30$, and $\varphi_0 = -\pi/2$. It is seen from the figure that the field distribution on the back face of the lens ($ky = 20$) is characterized by the presence of nonuniformly scaled intricate oscillations, which cannot be explained within the framework of GO. The distribution poorly resembles a uniform one, which is assumed in the calculation of the field in the focal region within the Kirchhoff approximation. Note in addition that the maximum field amplitude of such oscillations can exceed the field amplitude at the focus point (curve *3*).

We should emphasize that the transverse distribution of the field amplitude in the foal plain has a specific multilobe form and that distance D between the

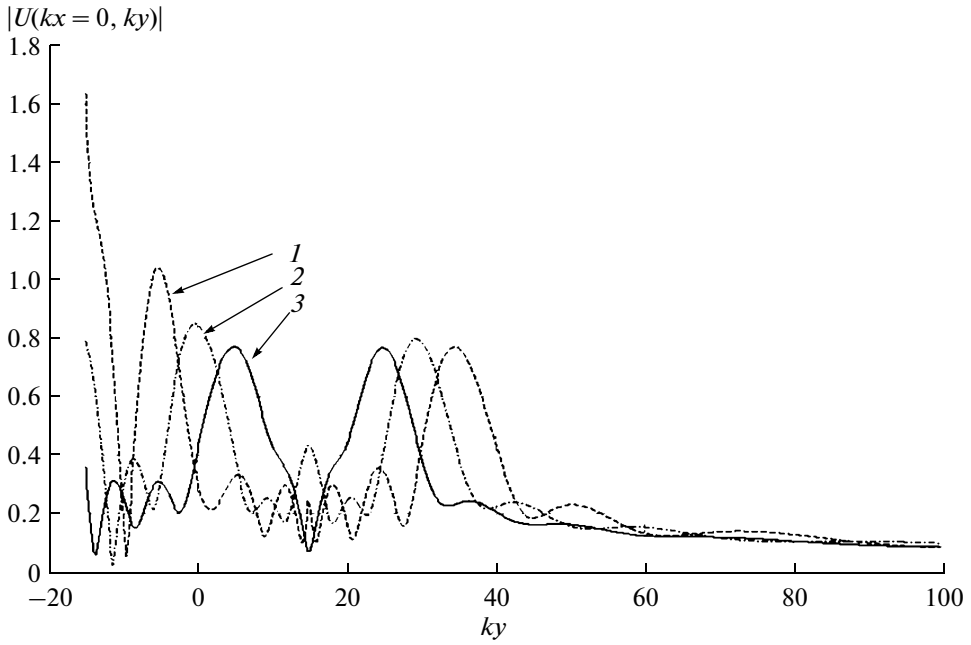

Fig. 8. Longitudinal distribution of the field on the lens axis for $\varepsilon = \mu = -1.0001$, $ka = 45$; $kb = 15$, and $\varphi_0 = -\pi/2$; $kR_0 = (1)$ 25, (*2*) 30, and (*3*) 35.

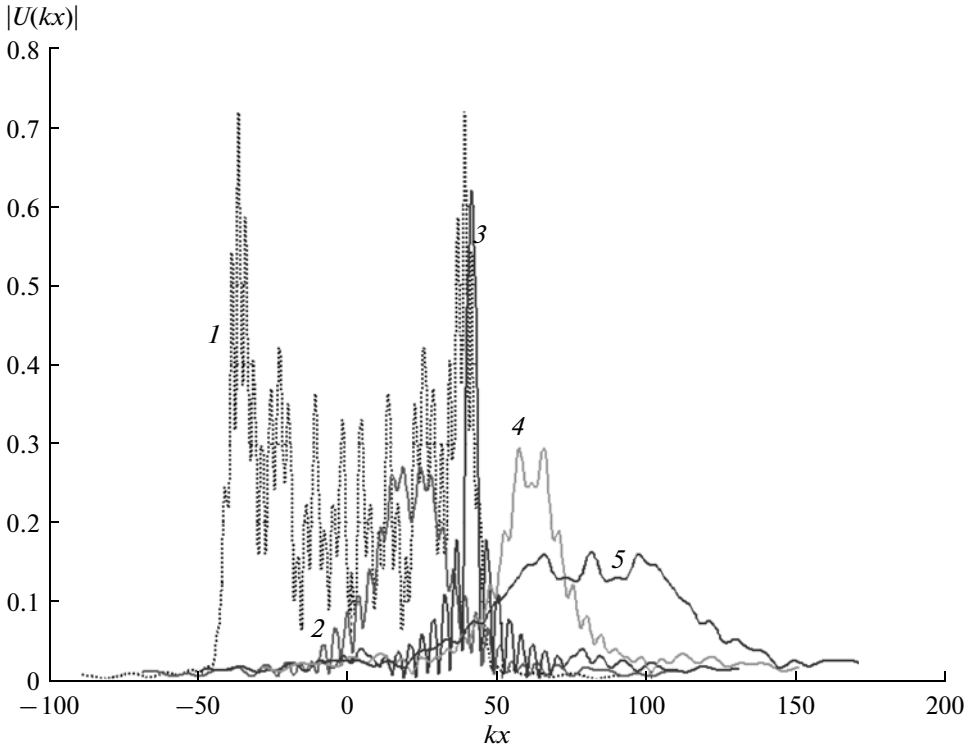

Fig. 9. Field distribution (curve *1*) on the upper face of the lens and in the planes $ky = \text{const}$ behind the lens for $\varepsilon = \mu = -1.0001$, $ka = 45$; $kb = 20$; $kR_0 = 30$, and $\varphi_0 = -\pi/2$; $ky = (2)$ 40, (*3*) 50, (*4*) 60, and (*5*) 80. Curves *2*–*5* are displaced along the *kx* axis by 20, 40, 60, and 80, respectively.

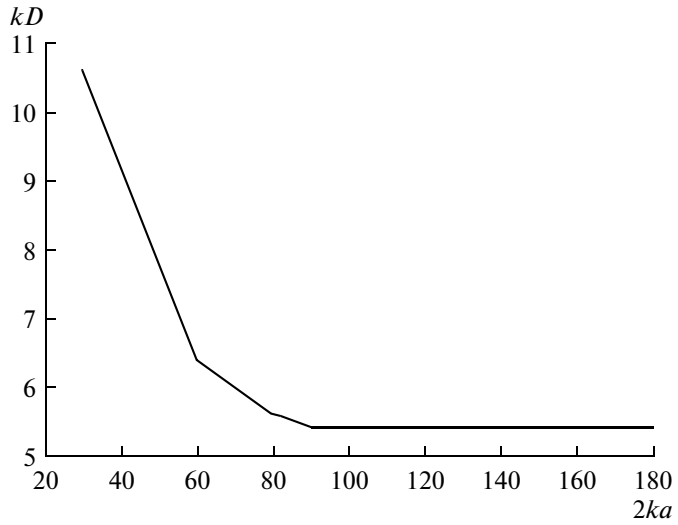

Fig. 10. Resolution of the lens vs. its length for $\varepsilon = \mu = -1.0001 - i \times 0.0001$; $2kb = 30$; $kR_0 = 25$, and $\varphi_0 = -\pi/2$.

neighboring minima bounding the main lobe exceeds $\lambda/2$. This proves the fact that the limit of the Rayleigh resolution cannot be exceeded in a thick Veselago lens.

Finally, Fig. 10 illustrates the calculated dependence of resolution D of the lens on its length $2ka$. It follows from the figure that, as the length grows, the resolution of the lens remains finite and satisfies the Rayleigh criterion.

Thus, the field behavior in the neighborhood of the focal point of a thick Veselago lens is the same as that for a standard lens, and the superresolution effect discussed in many publications is a myth.

2.3. The Electrodynamic Properties of a Thin Veselago Lens of Finite Dimensions

Let us present the results of computation of the problem of excitation of a plate with the electric dimensions

$$ka = 10; \quad (29)$$

$$kb = 1.00445. \quad (30)$$

We assume that the real parts of the relative permittivity and permeability of the metamaterial are

$$\varepsilon' = -1.000126, \quad (31)$$

$$\mu' = -0.990273, \quad (32)$$

and the imaginary parts of the permittivity and permeability of the metamaterial (the loss in the metamaterial medium) are $\varepsilon'' = 10^{-6}$ and $\mu'' = 10^{-6}$. We consider the case of the TM polarization of the incident cylindrical wave whose source Q has the coordinates $kR_0 = kb + 1$ and $\varphi_0 = -\pi/2$. Note that quantity σ characterizing the difference of ε' from minus unity is $\sigma = 6 \times 10^{-5}$. Thus, condition (23) is fulfilled and the lens can be regarded as a thin one. In addition, quantities ε', μ', and kb are chosen such that they provide for the degeneration of the even surface wave in an infinitely long layer (curve *1* from Fig. 3). This combination of parameters leads to resonance effects in the near field [25].

Figure 11 shows the calculated spatial distribution of the equal-amplitude lines for the total field. It follows from the figure that the field localizes near the upper ($-a \le x \le a$, $y = b$) and lower ($-a \le x \le a$, $y = -b$) faces of the plate. The spatial field distributions on the lower and upper faces of the plate have similar structures.

The structure of the near field is characterized by the presence of periodic oscillations, i.e., standing surface waves, whose maximum amplitudes monotonically decreases toward the narrow butt-ends of the

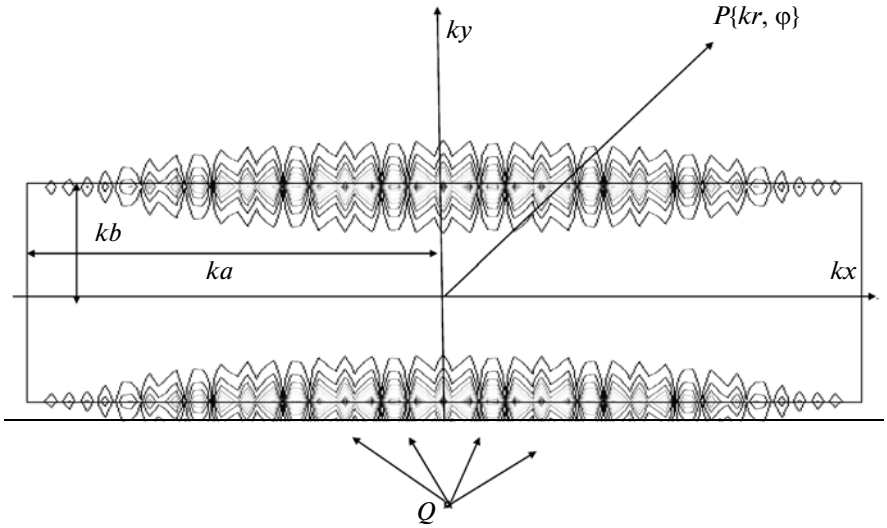

Fig. 11. Spatial distribution of equal-amplitude lines for the total field amplitude.

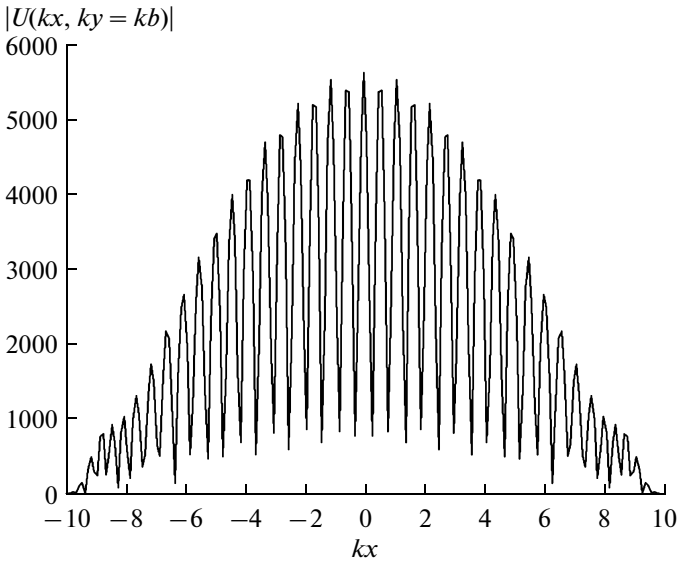

Fig. 12. Distribution of the total field amplitude over the upper face of the plate under the resonance conditions.

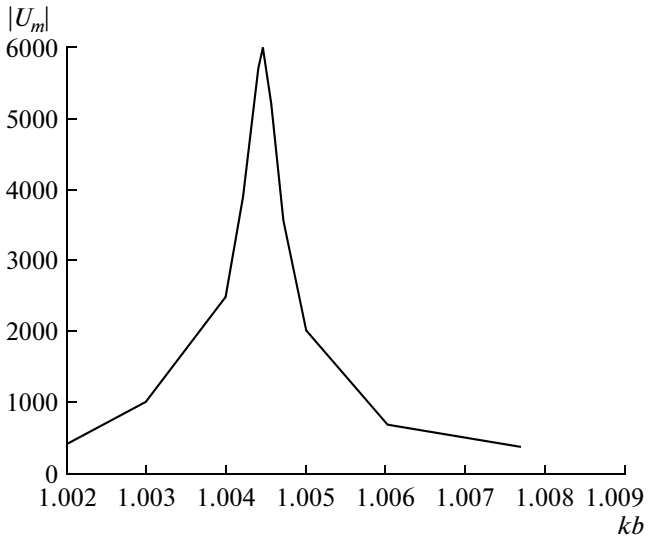

Fig. 13. Maximum total field amplitude at the center of the upper wide face of the plate vs. frequency.

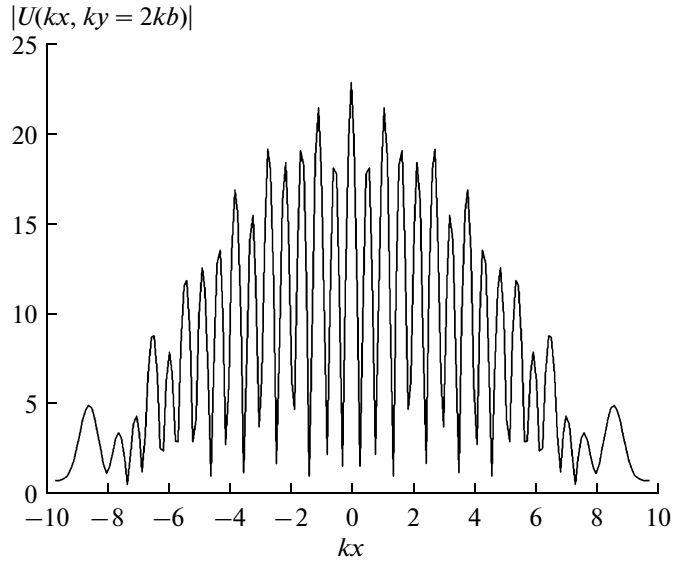

Fig. 14. Distribution of the total field amplitude in the focal plane under the resonance conditions.

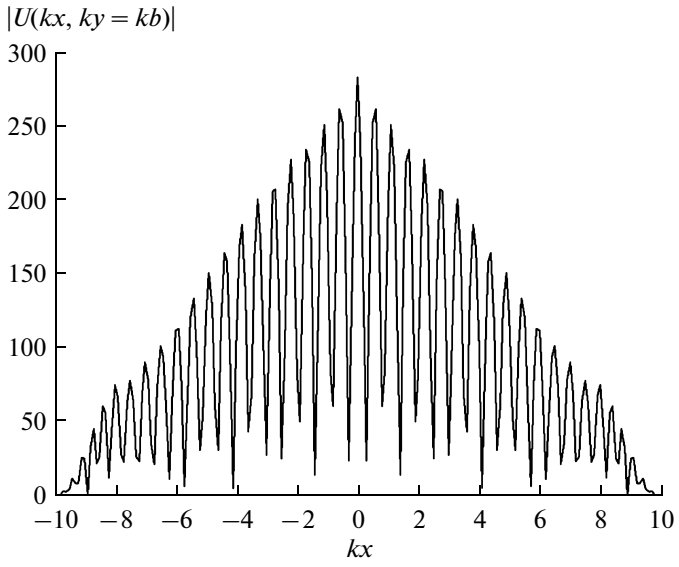

Fig. 15. Distribution of the total field amplitude over the upper face of the plate at a small distance from the resonance point.

plate. This is clearly seen from Fig. 12, which displays the distribution of $|U|$ over the upper face of the plate.

Figure 13 shows the frequency dependence of the absolute value of total field amplitude $U = |U(kb)|$ at the point $kx = 0$; $ky = kb$, i.e., at the center of the upper wide face of the plate, where the field has the maximum amplitude. Note that the distance from the lower wide face of the plate to cylindrical wave source Q is constant and equal to $kR_0 = kb + 1$. Frequency dependence $|U(kb)|$ from Fig. 13 has a resonance character, and the Q factor of the resonance is estimated by a quantity of about several thousand.

Figure 14 shows the field distribution in the focal plane ($ky = 2kb$) under the resonance conditions. The field amplitude takes its maximum value at the point that formally coincides with the focus point. The field amplitude at this point is smaller than the field intensity on the upper face of the plate by two orders of magnitude, and the field structure in the vicinity of the focus point fundamentally differs from the field structure at the analogous point for a thick lens (curve *3* from Fig. 9).

Figures 15 and 16 display the spatial field distributions on the upper face of the plate ($-a \le x \le a$, $y = b$)

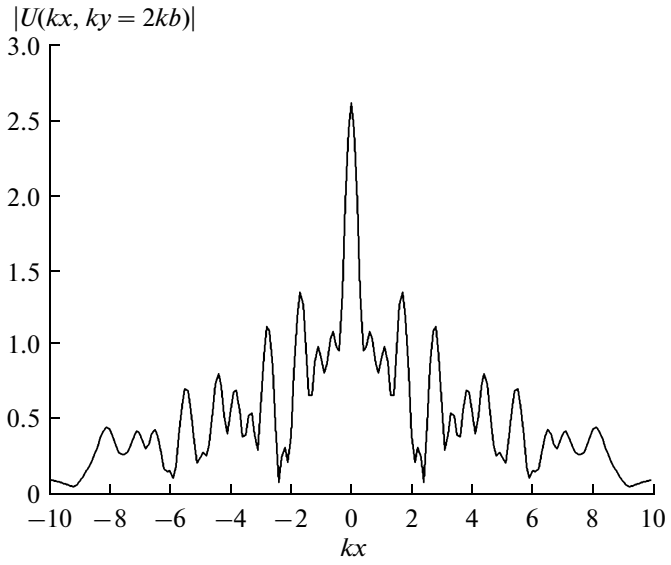

Fig. 16. Distribution of the total field amplitude in the focal plane at a small distance from the resonance point.

and in the focal plane ($-a \le x \le a$, $y = 2b$), respectively, when the value $ky = kb = 1$ differs from the resonance value $ky = kb = 1.00445$.

The comparison of the plots from Figs. 12 and 15 shows that the spatial field distribution on the upper face of the plate ($-a \le x \le a$, $y = b$) at a nonresonance point is similar to that in the case of the resonance point but has a substantially smaller amplitude.

For the focal plane, the character of the field distribution fundamentally differs from that observed in the case of the resonance point. This circumstance is manifested not only in the decrease of the field amplitude but also in the character of the field variation near the focus point $kx \approx 0$. Note that the character of the field variation near the focus point $kx \approx 0$ (see Fig. 16) substantially differs from the field behavior in the focus region for an electrically thick Veselago lens. Thus, the width of the main lobe is $kD \approx 0.8$, which indicates the presence of the superresolution effect that has the diffraction nature.

CONCLUSIONS

The results of rigorous calculation of the fields in the problem of diffraction of a cylindrical wave by a metamaterial layer (of a finite or an infinite dimension) have been analyzed for the case when the distance between the source and the boundary of the layer is smaller than its thickness and the values of electrodynamic parameters ε and μ are close to unity. According to the GO concepts, the field in this case should have two focuses: one focus in the interior and the other in the exterior of the layer. It has been shown that the spatial structures of the fields in thick and thin Veselago lenses (in which the layer thickness is substantially larger and smaller, respectively, than the wavelength) are significantly different. The field behavior in the neighborhood of the exterior focus of a thick lens coincides with that exhibited by standard lenses. The dimension of the spot in the focal plane cannot be smaller than $\lambda/2$. There is no superfocusing that consists in the violation of the Rayleigh criterion.

In thin Veselago lenses, the field is rather sensitive to the values of the layer parameters. In particular, high-Q resonances are observed. These resonances are characterized by an abrupt increase of the reactive field component, which cannot be described in terms of GO. Surface wave play a substantial role in the formation of the reactive field. The focusing effect that consists in the spatial field localization near the focal point does not occur. However, for a certain combination of parameters, the effect of diffraction superresolution can be observed. In this effect, the dimension of the diffraction spot in the focal plane is substantially smaller than $\lambda/2$.

Thus, with the help of a Veselago lens, it is impossible to transmit details of an image that are substantially smaller that the wavelength at a distance exceeding the wavelength.

ACKNOWLEDGMENTS

This study was supported by the Russian Foundation for Basic Research, project nos. 10-02-00053-a, 10-02-01103, and 12-02-00062-a.

REFERENCES

1. J. B. Pendry, Science **305** (5685), 788 (2004).
2. V. G. Veselago, Usp. Fiz. Nauk **92**, 517 (1967).
3. V. Veselago, L. Braginsky, V. Shklover, and C. J. Hafner, Comput. Theor. Nanoscie. **2**, 1 (2006).
4. A. V. Dorofeenko, A. A. Lisyansky, A. M. Merzlikin, and A. P. Vinogradov, Phys. Rev. **73**, 235126 (2006).
5. A. P. Anyutin, J. Radioelectron., No. 6 (2007) (http://ire/cplire.ru).
6. A. D. Shatrov, J. Commun. Technol. Electron. **52**, 1324 (2007).
7. A. P. Anyutin, J. Commun. Technol. Electron. **53**, 387 (2008).
8. A. P. Anyutin, J. Commun. Technol. Electron. **53**, 1323 (2008).
9. A. P. Anuytin, in *Metamaterials-2008 (Proc. 2nd Cong. on Advanced Electromagnetic Materials in Microwaves and Optics, Pamplona, Spain, Sept. 21–26, 2008)* (METAMORPHOSE, VI, AISBL, 2008), p. 21.
10. A. B. Petrin, JETP **107**, 364 (2008).
11. A. B. Petrin, JETP Lett. **87**, 464 (2008).
12. S. E. Bankov, J. Commun. Technol. Electron. **54**, 123 (2009).
13. A. P. Anyutin, Radiotekh. Elektron. (Moscow) **54**, 982 (2009).
14. A. P. Anyutin, in *Proc. Progress in Electromagnetic Research Symp. (PIERS), Moscow, Aug. 18–21, 2009*

(Electromagn. Academy, Cambridge, MA, 2009), p. 1036.
15. V. P. Mal'tsev and A. D. Shatrov, J. Commun. Technol. Electron. **55**, 278 (2010).
16. V. P. Mal'tsev and A. D. Shatrov, Fiz. Voln. Protsessov Radiotekh. Sist. **14** (3), 38 (2011).
17. A. S. Kryukovskii and D. S. Lukin, *Edge and Angular Catastrophes in the Uniform Geometric Theory of Diffraction* (MFTI, Moscow, 1999) [in Russian].
18. A. S. Kryukovskii, D. S. Lukin, E. A. Palkin, and D. V. Rastyagaev, J. Commun. Technol. Electron. **51**, 1087 (2006).
19. G. T. Markov and A. F. Chaplin, *Excitation of Electromagnetic Waves* (Radio i Svyaz', Moscow, 1983) [in Russian].
20. A. N. Logarkov and V. N. Kissel, Phys. Rev. Lett. **92**, 077401 (2004).
21. A. D. Yaghjian and T. B. Hansen, Phys. Rev. E **72**, 046608 (2006).
22. A. D. Shatrov, J. Commun. Technol. Electron. **52**, 842 (2007).
23. S. E. Bankov, *Electromagnetic Crystals* (Fizmatlit, Moscow, 2010) [in Russian].
24. V. P. Mal'tsev and A. D. Shatrov, J. Commun. Technol. Electron. **57**, 170 (2012).
25. A. P. Anyutin and A. D. Shatrov, J. Commun. Technol. Electron. **57**, 1024 (2012).
26. A. N. Lagarkov and V. N. Kisel', Dokl. Phys. **49**, 5 (2004).
27. A. P. Anioutine, A. G. Kyurkchan, and S. A. Minaev, J. Quant. Spectrosc. Radiat. Transfer **79–80**, 509 (2003).
28. A. G. Kyurkchan, S. A. Minaev, and A. L. Soloveichik, J. Commun. Technol. Electron. **46**, 615 (2001).

Translated by I. Efimova